PHYSICAL REVIEW D **91,** 042002 (2015)

Multimaterial coatings with reduced thermal noise

William Yam, Slawek Gras, and Matthew Evans
Massachusetts Institute of Technology, 185 Albany Street, Cambridge, Massachusetts 02139, USA
(Received 13 November 2014; published 3 February 2015)

The most sensitive measurements of time and space are made with resonant optical cavities, and these measurements are limited by coating thermal noise. The mechanical and optical performance requirements placed on coating materials, especially for interferometric gravitational wave detectors, have proven extremely difficult to meet despite a lengthy search. In this paper we propose a new approach to high performance coatings, the use of multiple materials at different depths in the coating. To support this we generalize previous work on thermal noise in two-material coatings to an arbitrary multimaterial stack, and develop a means of estimating absorption in these multimaterial coatings. This new approach will allow for a broadening of the search for high performance coating materials.

DOI: 10.1103/PhysRevD.91.042002 PACS numbers: 04.80.Nn

I. INTRODUCTION

Lasers and resonant optical cavities have become a ubiquitous tool in optical experiments which explore the bounds of physics through precise measurements of space and time [1–4]. The precision with which these measurements can be made is in large part determined by the fundamental thermal motion of the coatings used in optical resonators [5–7].

Interferometric gravitational wave detectors in particular set extremely stringent requirements on their coatings; they must simultaneously have good mechanical properties for low thermal noise, low optical absorption for high-power operation, and good surface figure to support multikilometer resonant cavities [8]. These requirements are, however, very hard to meet in a single material [9–20].

This paper provides the theoretical foundation for a new approach to the search for high quality coating materials. We compute the coating thermal noises and absorption which will result from coatings comprised of more than two materials. This is to be contrasted with previous works, which have assumed that optical coatings are made of one low-index material and one high-index material [21,22].

In the next section we present our model of coating Brownian and thermo-optic noises, generalized from previous works to allow for multimaterial coatings. We go on to develop a simple model of absorption as a function of depth in the coating, from which we are able to assess the impact of using relatively high absorption materials deep in the coating. These calculations are followed by a few examples of how this new approach can be used to produce coatings with lower thermal noise.

All frequently used symbols are given in Table I, and the Appendix connects the notation used in this work to that of previous authors.

II. MODEL OF COATING THERMAL NOISE

In order to elucidate the potential benefits of multimaterial coatings we will first describe briefly the model of thermal noise used in our calculations. For Brownian thermal noise we start with [21], and [22] is our starting point for thermo-optic noise, though similar treatments can be found in [23–25].

Since Hong *et al.* [21] conclude that changes in the ratio of shear to bulk mechanical loss do not significantly change the optimal coating design, and that photoelastic effects are relatively unimportant, we can simplify their result significantly by assuming that shear and bulk mechanical losses are equal, $\phi_M = \phi_{\text{bulk}} = \phi_{\text{shear}}$, and that the photoelastic effects can be ignored. (While not important for optimization, the ratio of shear and bulk losses impacts the level of Brownian thermal noise at the ±30% level [21].) The resulting equation for Brownian thermal noise is

$$S_z^{\text{Br}} = \frac{4k_B T}{\pi r_G^2 \omega} \frac{1-\sigma_s-2\sigma_s^2}{Y_s} \sum_j b_j d_j \phi_{Mj} \tag{1}$$

where the unitless weighting factor b_j for each layer is

$$b_j = \frac{1}{1-\sigma_j}\left[\left(1 - n_j \frac{\partial \phi_c}{\partial \phi_j}\right)^2 \frac{Y_s}{Y_j} + \frac{(1-\sigma_s-2\sigma_s^2)^2}{(1+\sigma_j)^2(1-2\sigma_j)} \frac{Y_j}{Y_s}\right].$$

Under the assumption that the substrate and coating elastic parameters are equal ($Y_j \to Y_s$ and $\sigma_j \to \sigma_s$), and ignoring field penetration into the coating ($\frac{\partial \phi_c}{\partial \phi_j} \to 0$), $b_j \to 2$ for all layers.

For thermo-optic noise we use

$$S_z^{\text{TO}} = \frac{4k_B T^2}{\pi r_G^2 \sqrt{2\kappa_s C_s \omega}} \left[\bar{\alpha}_c d - \bar{\beta}\lambda_0 - \frac{\bar{\alpha}_s}{C_s} \sum\nolimits_j d_j C_j\right]^2 \tag{2}$$

where

$$\bar{\alpha}_s = 2(1+\sigma_s)\alpha_s \tag{3}$$

TABLE I. Frequently used symbols for physical constants, the environment, material parameters, etc., are given above. Material parameters that appear with a subscript refer to either the substrate material, subscript s, the coating, subscript c, or are indexed to a particular coating layer, typically with the variable j. Note that k is occasionally used as a local index for summation or recursion when j is already in use.

Symbol	Name	Unit or value
k_B	Boltzmann's constant	1.38×10^{-23} J/K
T	Mean temperature	290 K
λ_0	Vacuum laser wavelength	1064 nm
k_0	laser wave number $= 2\pi/\lambda_0$	5.9×10^6/m
r_G	Gaussian beam radius ($1/e^2$ power)	6 cm
ω	Angular frequency	rad/s
S_z^{Br}	Brownian noise	m^2/Hz
S_z^{TO}	Thermo-optic noise	m^2/Hz
n	Refractive index	
α	Thermal expansion	1/K
β	$\partial n/\partial T$	1/K
κ	thermal conductivity	W/K m
C	Heat capacity per **volume**	$\mathrm{J/Km}^3$
Y	Young's Modulus	$\mathrm{N/m}^2$
σ	Poisson ratio	
ϕ_M	Mechanical loss angle	
a	Optical absorption	1/m
d	Coating thickness	m
z	Depth in the coating (negative)	m
P	Laser power arriving at each layer	W
E	Complex electric field amplitude	N/C
r	Complex amplitude reflectivity	
ρ	Power absorption ratio	
b	Brownian weight coefficient	

$$\bar{\alpha}_c = \sum_{j=1}^{N} \frac{d_j}{d} \frac{1+\sigma_s}{1-\sigma_j} \left[\frac{1+\sigma_j}{1+\sigma_s} + (1-2\sigma_s) \frac{Y_j}{Y_s} \right] \alpha_j \quad (4)$$

$$\bar{\beta} = \sum_{j=1}^{N} \frac{d_j}{\lambda_0} \left(\beta_j + \frac{1+\sigma_j}{1-\sigma_j} \alpha_j n_j \right) \frac{\partial \phi_c}{\partial \phi_j}. \quad (5)$$

Note that the expression for $\bar{\beta}$ is slightly different from that of [22], thanks to the correction by K. Yamamoto in Chap. 8.2.5 of [26].

In this paper we make a number of simplifying assumptions ($\phi_M = \phi_{\mathrm{bulk}} = \phi_{\mathrm{shear}}$, no photoelastic effect), and we ignore several correction factors (thick coating correction [22], finite size test-mass corrections [27,28]). All of this is to keep the formalism simple enough that the results can be easily understood and evaluated, but it should not be taken to mean that these corrections cannot be applied to multi-material coatings. Indeed, their application is expected to be a straightforward if somewhat messy process.

A. Reflection phase

In this section we summarize the model for coating reflectivity presented in Appendix B of [22], as this calculation forms the basis for computing the coating phase sensitivity to mechanical and thermal fluctuations [e.g., $\partial\phi_c/\partial\phi_j$ in Eqs. (1) and (5)]. In the next section, we extend this computation to include distributed absorption in coating materials, which is an essential ingredient in the primary result of this paper.

As in [22], we express the reflectivity of the interface between two coating layers, seen by a field moving from layer j to layer $j+1$ (see Fig. 1), as

$$r_j = \frac{n_j - n_{j+1}}{n_j + n_{j+1}}. \quad (6)$$

By recursively combining the interface reflectivities r_j, we can find the reflectivity of layer j and all of the layers between it and the substrate

$$\bar{r}_j = \frac{E_j}{E_j'} = e^{i\phi_j} \frac{r_j + \bar{r}_{j+1}}{1 + r_j \bar{r}_{j+1}}. \quad (7)$$

Note that while $\bar{r}_j$ includes the round-trip propagation phase in layer j, it does not include the reflectivity of the interface between layer $j-1$ and j.

The expression for $\bar{r}_j$ is recursive and the base case is the transition from the Nth coating layer to the substrate,

$$\bar{r}_N = e^{i\phi_N} r_N \quad (8)$$

which can be evaluated with (6) using $n_{N+1} = n_s$. Total coating reflectivity $\bar{r}_0$ is evaluated with the external vacuum acting as layer zero such that $n_0 = 1$.

The sensitivity of the coating reflection phase to a change in layer j

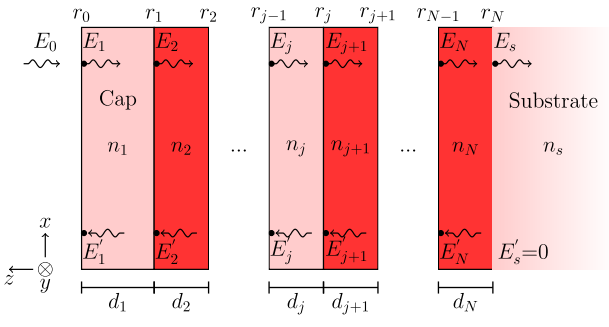

FIG. 1 (color online). The numbering of coating layers, interfaces and fields is shown above. The z-coordinate is zero at the coating surface, and is positive moving away from the coating. Note that the E-fields are evaluated just inside each coating layer (e.g., E_1 is evaluated at $z = -\epsilon$ in the limit of $\epsilon \to 0$).

$$\frac{\partial\phi_c}{\partial\phi_j} = \mathrm{Im}\left[\frac{1}{\bar{r}_0}\frac{\partial\bar{r}_0}{\partial\phi_j}\right] = \mathrm{Im}\left[\frac{\partial \log \bar{r}_0}{\partial\phi_j}\right] \tag{9}$$

is given by the recursion relation

$$\frac{\partial\bar{r}_k}{\partial\phi_j} = \begin{cases} e^{i\phi_k}\frac{1-r_k^2}{(1+r_k\bar{r}_{k+1})^2}\frac{\partial\bar{r}_{k+1}}{\partial\phi_j} & k<j \\ i\bar{r}_k & k=j \\ 0 & k>j \end{cases} \tag{10}$$

with the recursion starting at $k=0$, progressing through increasing values of k, and terminating at $k=j$.

B. Optical absorption

Maintaining extremely low optical absorption in high-reflection coatings severely limits the choice of coating materials [29]. The key idea behind this paper and its experimental counterpart [30], is that this stringent requirement need not be applied to all layers in the coating, but only to those near the surface which are dominantly responsible for the absorption of the coating. This is true for both the input coupler and end mirror of any high-finesse cavity, since the power inside the cavity is much higher than either the incident or transmitted power.

To compute the depth dependence of optical absorption in a coating, we start by evaluating the electric field present in each layer of the coating

$$E_{j+1} = \frac{\sqrt{1-r_j^2}}{1+r_j\bar{r}_{j+1}}E_j \tag{11}$$

(see Fig. 1). This expression can be used iteratively to compute the field entering each coating layer given that the field entering the coating from the vacuum is $E_0 = \sqrt{2P_0/\pi r_G^2 c\epsilon_0}$, where P_0 is the power of the incident laser beam, while c and ϵ_0 are the speed of light and the permittivity of free space (see [21] or Appendix A of [31]).

The field at any point in a given layer will be the sum of the two counterpropagating fields

$$E(z_j,t) = \mathrm{Re}[E_j e^{i(\omega t + k_0 n_j z_j)} + E'_j e^{i(\omega t - k_0 n_j z_j)}] \tag{12}$$

$$\text{where } z_j = z - \textstyle\sum_{k=1}^{j-1} d_k \tag{13}$$

such that $z_j = 0$ at the top of layer j, and $z_j = -d_j$ at the bottom. Optical absorption per unit length in a layer is assumed to be proportional to the time averaged field amplitude squared integrated over that layer, normalized by the power entering the layer and the layer thickness

$$\rho_j = \frac{2}{|E_j|^2 d_j}\left\langle \int_{-d_j}^{0} E(z_j,t)^2 dz_j \right\rangle_t \tag{14}$$

$$= (1+|\bar{r}_j|^2) + 2\frac{\sin(k_0 n_j d_j)}{k_0 n_j d_j}\mathrm{Re}[\bar{r}_j e^{ik_0 n_j d_j}]. \tag{15}$$

TABLE II. The values of material parameters used for all figures and examples. The values for SiO_2 and Ta_2O_5 are taken from [22], while those of the hypothetical metal-oxides MO_A and MO_B have been invented by the authors for use in examples presented in the text.

Property	SiO_2	Ta_2O_5	MO_A	MO_B	Unit
n	1.45	2.1	2.1	3.0	1
α	0.51	3.6	3.0	3.0	10^{-6}/K
β	8	14	10	10	10^{-6}/K
κ	1.38	33	30	30	W/m K
C	1.64	2.1	2.0	2.0	MJ/K × m^3
Y	72	140	100	70	GPa
σ	0.17	0.23	0.2	0.2	1
ϕ_M	0.4	3.8	1.0	1.0	10^{-4}
a	10^{-3}	2	10	100	ppm/μm

Note that the second term is zero for quarter-wave layers (i.e., with $k_0 n_j d_j = \pi/2$), and that ρ_j is constructed such that $\rho_j = 1$ for $\bar{r}_j = 0$ (i.e., for a field propagating in the absence of a counterpropagating field).

Using Eq. (11) we can further relate the absorption in each layer to the total absorption coefficient for the coating a_c, by

$$a_c = \sum_{j=1}^{N}\bar{\rho}_j a_j d_j \quad \text{where } \bar{\rho}_j = \frac{|E_j|^2}{|E_0|^2}\rho_j \tag{16}$$

and a_j is the absorption per unit length of the material used in layer j.

Absorption loss in coatings is usually quoted as a single value, the total a_c, rather than an absorption per unit length for the coating constituents [17,20]. Using Eq. (16) we can convert absorption values in the literature into absorption per unit length. Assuming that odd layers are SiO_2 with negligible absorption,

$$a_X = \frac{1}{a_c}\sum_{j=\text{even}}^{N}\bar{\rho}_j d_j \tag{17}$$

which we use to compute the value for Ta_2O_5 presented in Table II.

III. EXAMPLE COATINGS

Given the coating model described in the previous section, and a pallet of possible coating materials, we can evaluate the impact of using more than two materials to make a coating. In this paper we allow ourselves two hypothetical coating materials, metal-oxide A and B (MO_A and MO_B) as a means of demonstrating the types of optimizations which can occur (see Table II).

The coating examples presented in this section are designed to show how multimaterial coatings can *in*

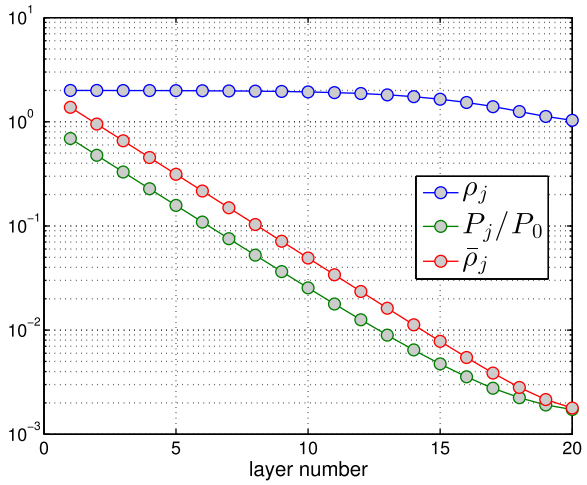

FIG. 2 (color online). The contribution of coating layers to the total coating absorption varies with depth in the coating. Deeper layers make a smaller contribution, as seen by the rapidly decreasing value of $\bar{\rho}_j$ with increasing j. The two ingredients of $\bar{\rho}$, absorption of each layer relative to the power arriving at that layer, ρ_j, and power attenuation as a function of depth P_j/P_0, are also shown [see Eqs. (14)–(16)]. The coating used to generate this figure consists of 10 SiO_2-Ta_2O_5 quarter-wave doublets.

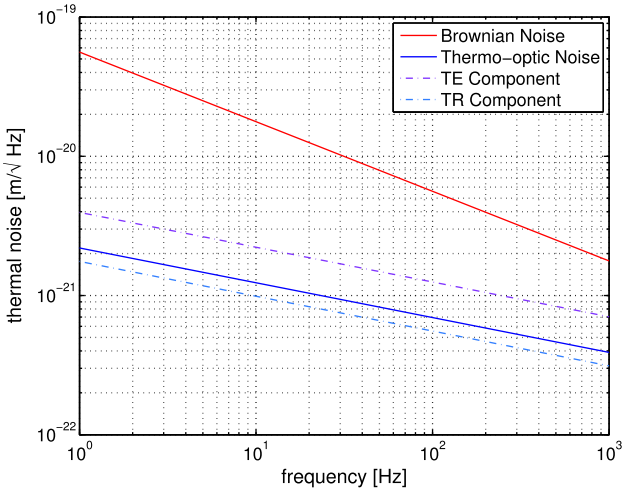

FIG. 4 (color online). Brownian thermal noise dominates in this example coating, in part thanks to the cancellation of the thermo-elastic (TE) and thermo-refractive (TR) components of thermo-optic noise. The noise level of 4.6×10^{-21} m/$\sqrt{\text{Hz}}$ at 100 Hz is a useful benchmark for the impact of coating thermal noise on gravitational wave detectors. The coating used to generate this figure consists of 10 SiO_2-Ta_2O_5 quarter-wave doublets.

principal be used to produce low-noise coatings. For a detailed application of this approach to three-material coatings involving amorphous silicon see [30].

As a baseline, we start by computing the thermal noise seen by 1064 nm light for a 20-layer coating, made of 10 SiO_2-Ta_2O_5 layer pairs or "doublets." The top layer, known as the "cap" has an optical thickness equal to half of the laser wavelength, such that $d_1 n_1/\lambda_0 = \frac{1}{2}$. All of the deeper coating layers are quarter wave with $d_j n_j/\lambda_0 = \frac{1}{4}$. The results of calculations for this coating are shown in Figs. 2, 3 and 4. This coating transmits 0.1% of the incident light power, and absorbs 0.5 ppm.

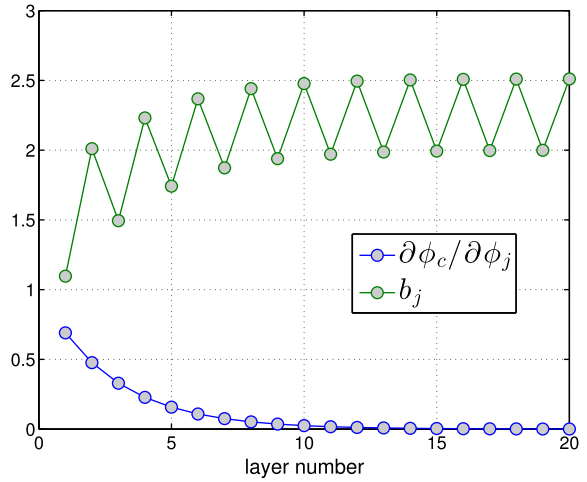

FIG. 3 (color online). The contribution of coating layers to Brownian noise increases with depth in the coating. This figure shows the coating phase sensitivity to fluctuations in each layer, $\partial\phi_c/\partial\phi_j$, and the weight of each layer in the total Brownian noise, b_j [see Eqs. (1) and (9)].

For comparison, we can change the high-index material used below the top 3 coating doublets to MO_A, which is similar to Ta_2O_5 but is somewhat softer, has lower mechanical loss, and much higher absorption. The lower Young's modulus makes a better match to the SiO_2 substrate, and combines with the lower ϕ_M to reduce the Brownian noise of this coating to 70% of the baseline coating. The transmission of this coating is the same as the baseline, and the absorption is only slightly higher at 0.6 ppm.

A more extreme example is a coating made of 4 SiO_2-Ta_2O_5 doublets, and 3 SiO_2-MO_B doublets. This coating has less than 70% of the Brownian noise of the baseline coating, and only 0.8 ppm absorption. The high refractive index of this material means that fewer and thinner layers are needed relative to Ta_2O_5 to produce the same transmission. This, in combination with the good mechanical properties of this coating, more than compensate for its high absorption of 100 ppm/μm.

IV. CONCLUSIONS

Precision optical measurements are increasingly limited by coating thermal noise, and much time and effort has been and continues to be spent in the search for better coating materials [5]. In this work we suggest that the search for coating materials should not focus on finding a

single material which satisfies all requirements, but rather a pallet of materials which together can be used to make coatings which satisfy all requirements.

While a single high-index, low absorption and low mechanical loss material would be ideal, the examples in this work show that a high-index material with low mechanical loss, but not necessary low optical absorption, will suffice to make lower noise coatings possible. Since the material properties of a given coating layer depend not only on its constituents (e.g., doping), but also on the manufacturing process (e.g., annealing) a wide range of material properties have already been measured or are potentially accessible.

ACKNOWLEDGMENTS

The authors gratefully acknowledge the support of the National Science Foundation and the LIGO Laboratory, operating under Cooperative Agreement No. PHY-0757058.

APPENDIX: RELATION TO OTHER WORKS

The expressions in this work are related to those of [21] by

$$\bar{r}_0 = \rho_{\mathrm{tot}} \tag{A1}$$

$$2\frac{\partial \phi_c}{\partial \phi_j} = \mathrm{Im}\left[\frac{\partial \log \rho}{\partial \phi_j}\right] \;\forall\; 1 \le j \le N \tag{A2}$$

$$= \mathrm{Im}[\epsilon_j/n_j] \text{ for their } \beta_j = 0 \tag{A3}$$

with our expression on the left of each equality and theirs on the right. The factor of 2 results form our definition of ϕ_j as a **round-trip** phase in each layer, while theirs is a one-way phase.

We did, however, follow the convention of [21] for the direction of the z-axis: normal to the surface of the coating and pointing *into* the vacuum. This represents a sign reversal relative to [22], such that $\partial\phi_c/\partial\phi_j$ is generally positive in this work as in [21].

An earlier treatment of Brownian thermal noise which included field penetration effects was performed in [24]. They based their computation on the coating reflection phase sensitivity to interface displacements (rather than layer thickness changes) and their notation is connected to ours by

$$n_j\frac{\partial \phi_c}{\partial \phi_j} - n_{j+1}\frac{\partial \phi_c}{\partial \phi_{j+1}} = \epsilon_j \tag{A4}$$

again with our expression on the left of the equality and theirs on the right.

[1] D. E. McClelland, N. Mavalvala, Y. Chen, and R. Schnabel, Laser Photonics Rev. **5**, 677 (2011).
[2] R. Schnabel, N. Mavalvala, D. E. McClelland, and P. K. Lam, Nat. Commun. **1**, 121 (2010).
[3] M. Poot and H. S. J. van der Zant, Phys. Rep. **511**, 273 (2012).
[4] G. Zavattini, U. Gastaldi, R. Pengo, G. Ruoso, F. D. Valle, and E. Miotti, Int. J. Mod. Phys. A **27**, 1260017 (2012).
[5] T. Kessler, C. Hagemann, C. Grebing, T. Legero, U. Sterr, F. Riehle, M. J. Martin, L. Chen, and J. Ye, Nat. Photonics **6**, 687 (2012).
[6] G. D. Cole, W. Zhang, M. J. Martin, J. Ye, and M. Aspelmeyer, Nat. Photonics **7**, 644 (2013).
[7] R. Adhikari, Rev. Mod. Phys. **86**, 121 (2014).
[8] P. Fritschel, arXiv:1411.4547.
[9] D. Crooks, P. Sneddon, G. Cagnoli, J. Hough, S. Rowan, M. M. Fejer, E. Gustafson, R. Route, N. Nakagawa, and D. Coyne, Classical Quantum Gravity **19**, 883 (2002).
[10] G. M. Harry, A. M. Gretarsson, P. R. Saulson, S. E. Kittelberger, S. D. Penn, W. J. Startin, S. Rowan, M. M. Fejer, D. Crooks, and G. Cagnoli, Classical Quantum Gravity **19**, 897 (2002).
[11] K. Yamamoto, M. Ando, K. Kawabe, and K. Tsubono, Phys. Lett. A **305**, 18 (2002).
[12] S. D. Penn *et al.*, Classical Quantum Gravity **20**, 2917 (2003).
[13] E. D. Black, A. Villar, K. Barbary, A. Bushmaker, J. Heefner, S. Kawamura, F. Kawazoe, L. Matone, S. Meidt, S. R. Rao, K. Schulz, M. Zhang, and K. G. Libbrecht, Phys. Lett. A **328**, 1 (2004).
[14] D. R. M. Crooks, G. Cagnoli, M. M. Fejer, G. Harry, J. Hough, B. T. Khuri-Yakub, S. Penn, R. Route, S. Rowan, P. H. Sneddon, I. O. Wygant, and G. G. Yaralioglu, Classical Quantum Gravity **23**, 4953 (2006).
[15] G. M. Harry, H. Armandula, E. Black, D. Crooks, G. Cagnoli, J. Hough, P. Murray, S. Reid, S. Rowan, and P. Sneddon, Appl. Opt. **45**, 1569 (2006).
[16] G. M. Harry *et al.*, Classical Quantum Gravity **24**, 405 (2007).
[17] M. R. Abernathy, G. M. Harry, F. Travasso, I. Martin, S. Reid, S. Rowan, J. Hough, M. M. Fejer, R. Route, S. Penn, H. Armandula, and A. Gretarsson, Phys. Lett. A **372**, 87 (2008).
[18] I. Martin *et al.*, Classical Quantum Gravity **25**, 055005 (2008).
[19] I. W. Martin *et al.*, Classical Quantum Gravity **26**, 155012 (2009).
[20] R. Flaminio, J. Franc, C. Michel, N. Morgado, L. Pinard, and B. Sassolas, Classical Quantum Gravity **27**, 084030 (2010).
[21] T. Hong, H. Yang, E. Gustafson, R. Adhikari, and Y. Chen, Phys. Rev. D **87**, 082001 (2013).

[22] M. Evans, S. Ballmer, M. Fejer, P. Fritschel, G. Harry, and G. Ogin, Phys. Rev. D **78**, 102003 (2008).
[23] M. L. Gorodetsky, Phys. Lett. A **372**, 6813 (2008).
[24] A. Gurkovsky and S. Vyatchanin, Phys. Lett. A **374**, 3267 (2010).
[25] N. M. Kondratiev, A. G. Gurkovsky, and M. L. Gorodetsky, Phys. Rev. D **84**, 022001 (2011).
[26] G. Harry, T. P. Bodiya, and R. DeSalvo, *Optical Coatings and Thermal Noise in Precision Measurement* (Cambridge University Press, Cambridge, 2012).
[27] V. B. Braginsky and S. P. Vyatchanin, Phys. Lett. A **312**, 244 (2003).
[28] K. Somiya and K. Yamamoto, Phys. Rev. D **79**, 102004 (2009).
[29] F. Beauville *et al.*, Classical Quantum Gravity **21**, S935 (2004).
[30] J. Steinlechner, I. W. Martin, J. Hough, C. Krueger, S. Rowan, and R. Schnabel, Phys. Rev. D **91**, 042001 (2015).
[31] P. Kwee, J. Miller, T. Isogai, L. Barsotti, and M. Evans, Phys. Rev. D **90**, 062006 (2014).